The Astrophysical Journal Letters, 925:L15 (10pp), 2022 February 1 https://doi.org/10.3847/2041-8213/ac4bd5

The Asteroid 162173 Ryugu: a Cometary Origin

Hitoshi Miura[1], Eizo Nakamura[2,3], and Tak Kunihiro[2]
[1] Department of Information and Basic Science, Nagoya City University, Nagoya, Japan
[2] The Pheasant Memorial Laboratory, Institute for Planetary Materials, Okayama University, Misasa, Japan
[3] Advanced Science Research Center, Okayama University, Misasa, Japan
Received 2021 October 11; revised 2021 December 28; accepted 2022 January 15; published 2022 January 31

Abstract

The Japanese Hayabusa2 mission has revealed in detail the physical characteristics of the C-type asteroid 162173 Ryugu, in particular, its spinning top-shaped rubble-pile structure and potentially high organic content. A widely accepted formation scenario for Ryugu is catastrophic collision between larger asteroids and the subsequent slow gravitational accumulation of collisional debris. An alternative scenario is that Ryugu is an extinct comet that lost its icy components. Here, we numerically simulated the sublimation of water ice from a porous cometary nucleus until the refractory components, such as silicate rocks and organic matter, were left behind as evaporative residues. Such a process represents the transformation from a comet to an asteroid. The spin-up related to the shrinking nucleus, associated with water ice sublimation, was also calculated. The result of the calculation indicates that the cometary origin scenario can account for all the features of Ryugu discussed above. We conclude that organic-rich spinning top-shaped rubble-pile asteroids, such as Ryugu, are comet–asteroid transition objects or extinct comets.

Unified Astronomy Thesaurus concepts: Asteroids (72); Comets (280)

1. Introduction

Sample return missions represent great opportunities to study materials from known locations on objects other than the Earth. The Hayabusa mission returned material to Earth from the asteroid Itokawa in 2010 (Fujiwara et al. 2006) and revealed through geochemistry that the asteroid was genetically related to ordinary chondrites (Nakamura et al. 2012, e.g.,). The following Hayabusa2 mission returned material from Ryugu to Earth on 2020 December 6 (Watanabe et al. 2019) and the OSIRIS-REx mission is expected to return samples from another asteroid, Bennu, in 2023 (Lauretta et al. 2019). Both Ryugu and Bennu are C-type asteroids and are considered to be genetically related to carbonaceous chondrites. The aforementioned sample return missions are expected to dramatically advance our understanding of the processes affecting the formation and evolution of bodies within the solar system along with the origin of prebiotic organic matter by performing a detailed comprehensive geochemical analysis of the returned samples with state-of-the-art analytical equipment on Earth.

The Hayabusa2 mission has revealed three major features of the asteroid Ryugu based on the proximity remote-sensing observations. The first feature is a rubble-pile structure. Because of the high porosity and the large boulders on the surface of Ryugu, the interior was considered to consist of boulders weakly agglomerated gravitationally (Watanabe et al. 2019), similar to Itokawa as investigated by the predecessor Hayabusa mission (Fujiwara et al. 2006). It has been proposed that the rubble-pile structure was formed by the re-accumulation of collisional debris after catastrophic collision between larger asteroids (Michel et al. 2001; Walsh 2018). The second feature is its spinning top shape, which suggests a rotation-induced deformation. The spin period required for the deformation is estimated to be about 3.5 hr, below which the centrifugal force exceeds the gravitational force at the equatorial plane of the object (Watanabe et al. 2019). In the scenario with accretion of collisional debris, numerical simulations supported that the spinning top shape is the consequence of the angular momentum gained during re-accumulation (Michel et al. 2020). The third feature is its high organic matter content. Mass-balance calculations based on the difference in albedo between the surface and the underground materials recognized after the touchdown of the Hayabusa2 spacecraft inferred that the surface layer of Ryugu would contain about 60% organic matter by area, if the coexisting silicate components have optical properties similar to those of CM chondrites (Potiszil et al. 2020). This estimate is much larger than the typical organic content in carbonaceous chondrites (Kerridge 1985, likely <10 wt. %). It has also been pointed out that the low thermal inertia and bulk density of Ryugu may be due to its high organic content (Okada et al. 2020). The re-accumulation scenario explains the first and second features but not the third one if the organic content of Ryugu samples is much greater than that of carbonaceous chondrites.

An alternative scenario, which can satisfy the three major features of the asteroid Ryugu simultaneously, is a cometary origin (Nakamura et al. 2019; Potiszil et al. 2020). Comets are small bodies formed at the outer cold region of the solar system and mainly composed of water ice and slightly less extent rocky components (debris). If such comets enter the inner solar system due to some dynamical effect, they are heated by solar irradiation and subsequently, the water ice sublimates, leaving rocky debris behind that finally transforms into a compact, rubble-pile asteroid. The ice sublimation also causes spin-up of the comet due to the shrinkage of the nucleus and the consequent decrease in the moment of inertia (Watanabe 1992). As a result of the spin-up, the cometary nucleus may have acquired the fast rotation required for the formation of the spinning top shape. In addition, the ice components of comets are expected to contain a fraction of organic matter that formed in the interstellar medium (Ehrenfreund & Charnley 2000;

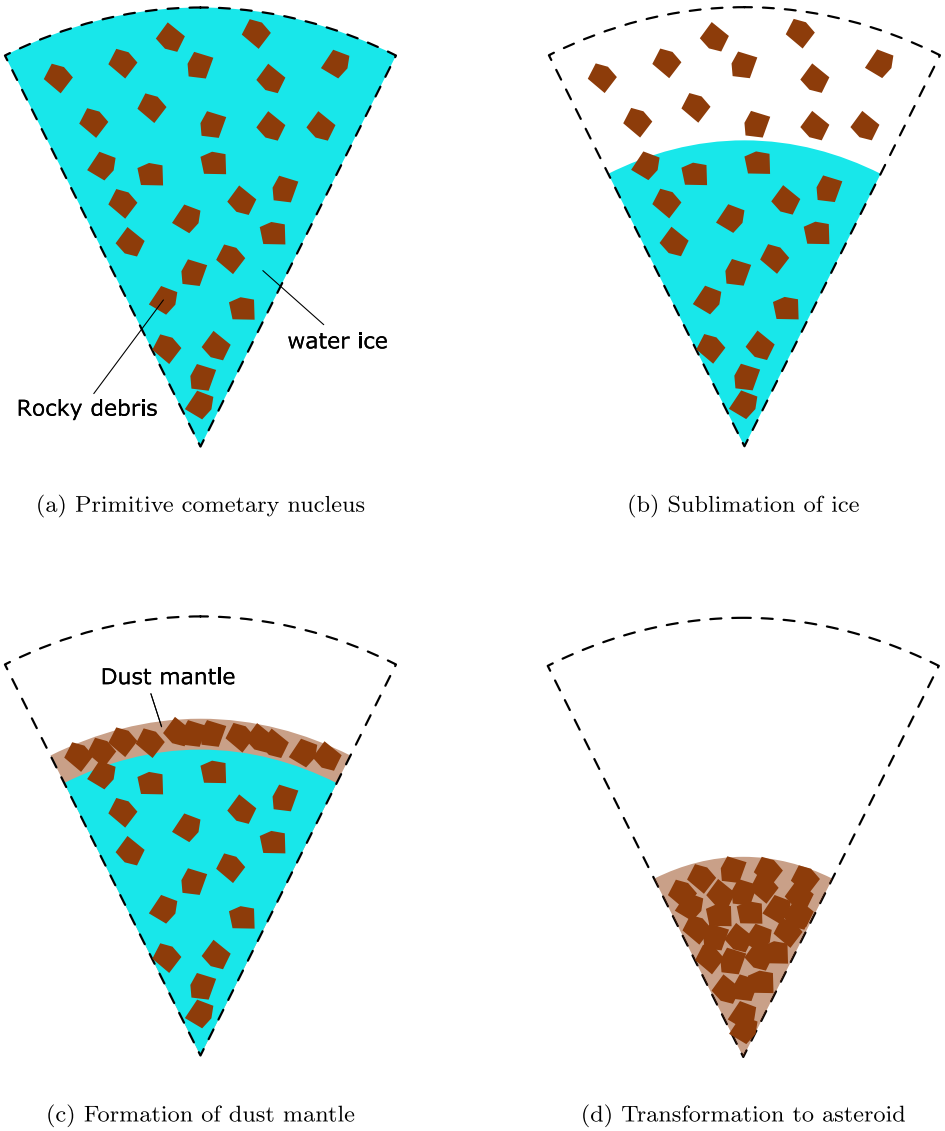

(a) Primitive cometary nucleus

(b) Sublimation of ice

(c) Formation of dust mantle

(d) Transformation to asteroid

Figure 1. A model of water ice sublimation from a porous cometary nucleus. (a) The cometary nucleus is initially assumed to consist mainly of water ice particles with a small amount of rocky debris uniformly contained within. (b) The water ice sublimates from the outer layer and the primitive region shrinks. (c) The remaining rocky debris accumulates on the surface to form a dust mantle. Since the dust mantle is highly porous and therefore permeable, the water vapor generated inside leaks out through the dust mantle. (d) Finally, the cometary nucleus transforms to a rocky asteroid after almost complete sublimation of water ice.

Ehrenfreund & Schutte 2000). The refractory organic matter will be deposited, filling the space between the rocky debris as an organic residue layer after the water ice sublimates.

However, it is unknown how long it takes for the ice to sublimate completely, and how much the body will eventually spin-up by. In order to verify the cometary origin scenario of Ryugu, a numerical simulation was undertaken in which the ice is sublimated from a cometary nucleus until it transforms to a rubble-pile asteroid.

2. Model

Figure 1 shows the outline of our model. Let us consider a uniform, spherically symmetric, highly porous cometary nucleus composed of μm-sized water ice particles and cm-sized rocky debris. As the water ice sublimates from the outer layer of the nucleus, the remaining rocky debris piles up on the surface to form a dust mantle. The dust mantle is also highly porous and therefore permeable, allowing the sublimation of water ice from inside. As the water ice continues to sublimate, the cometary nucleus shrinks and eventually becomes a compact, rubble-pile asteroid consisting only of rocky debris. Although an individual ice particle contains a silicate core in the center, we do not consider the silicate core because most such sub-μm-sized particles are expected to be entrained with the escaping water vapor and finally ejected from the nucleus (see Appendix B). In addition, in this model, we deal with the sublimation only of the water that exists as independent ice, and do not consider that stored in hydrated silicates.

We derived an analytical solution of the pressure distribution of water vapor in the interior of the cometary nucleus with a two-layered structure of the inner primitive region and the outer dust mantle, and used it to determine the contraction rate of the nucleus. In order to obtain the time until the water ice sublimates completely (sublimation time), the time evolution equation for the radius of the cometary nucleus was numerically integrated until the radius of the primitive region became zero. We also calculated the change in the spin rate of

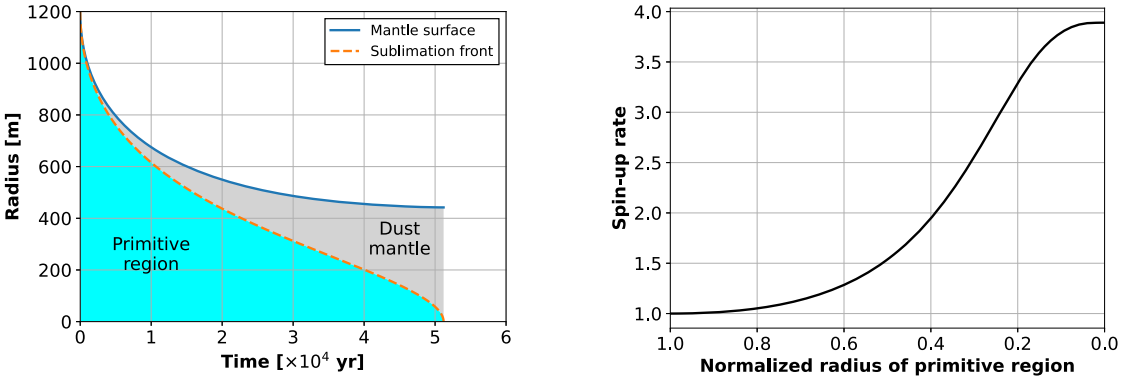

(a) Shrinkage of cometary nucleus (b) Spin-up of cometary nucleus

Figure 2. Numerical results. (a) The shrinkage of the cometary nucleus due to water ice sublimation. The time variations of the radii of the primitive region and the dust mantle are shown by dashed and solid curves, respectively. (b) The change in angular velocity of the cometary nucleus associated with the shrinkage due to water ice sublimation. The spin-up rate in the vertical axis is the angular velocity when the radius of the primitive region contracts to the value given by the horizontal axis as the ratio with respect to the initial angular velocity.

the cometary nucleus as it contracts, and determined how much the angular velocity can be amplified relative to the pre-sublimation state. Watanabe (1992) formulated the spin-up associated with the contraction of a cometary nucleus, but it was based on the assumption that the contraction is sufficiently small relative to the initial radius. We have extended Watanabe's formulation to apply to the drastic transformation from comet to asteroid. Details of our formulation are described in Appendix A.

3. Results

Figure 2(a) shows the time evolution of the radius of the cometary nucleus over time with the initial radius being 1.2 km. The initial water/rock-mass ratio is assumed to be 3 as expected from the solar system abundance (Hayashi 1981). The icy particles and rocky debris are assumed to be spheres with radii of 1 μm and 1 cm, respectively, and both are randomly packed in the primitive region, while the dust mantle is occupied by rocky debris only. As the water ice sublimates, the rocky debris left behind accumulates on the surface of the nucleus to keep the macroporosity at a constant value, assumed to be 0.6 in this study. The temperature inside the nucleus is assumed to be homogeneous at 200 K. The rationale for the values given above is described in Appendix A. Figure 2(a) demonstrates the rapid shrinkage of the primitive region and simultaneously the increase in the thickness of the dust mantle as the water ice sublimates. It took about 8 yr for the dust mantle to reach a thickness of 1 m, and about 640 yr to reach 10 m. The sublimation rate decayed as the dust mantle grew, and it took about 51 kyr for the water ice to sublimate completely. The thickness of the final dust mantle, i.e., the radius of the rubble-pile asteroid, is 442 m, which is approximately equal to the radius of present-day Ryugu (about 420 m).

Figure 2(b) shows the change in the angular velocity associated with the contraction of the cometary nucleus. The radius of the primitive region halves in about 11 kyr, and the angular velocity is gradually increasing. As the water ice sublimation progresses and the dust mantle growth becomes more pronounced, the angular velocity increases rapidly. The spin acceleration is due to the fact that the decrease in the moment of inertia of the cometary nucleus is more remarkable than the angular momentum loss by the release of water vapor. The angular velocity eventually increases to about 3.9 times the initial value.

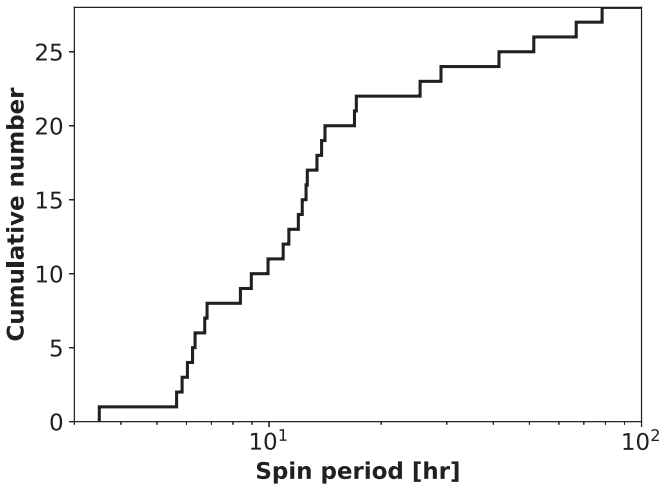

Figure 3. The distribution of spin periods of 28 cometary nuclei measured so far. The data is compiled from observational results in the literature (Huebner et al. 2006; Samarasinha et al. 2019). The vertical axis represents the cumulative number of cometary nuclei with a spin period shorter than the value given by the horizontal axis.

4. Discussions

A major question concerning the current study is whether the cometary nucleus is able to achieve the angular velocity necessary to reproduce Ryugu's spinning top shape. The model outlined so far contains only a mechanism to amplify the initial rotation of the cometary nucleus. In other words, we need information on the initial angular velocity of the cometary nucleus, which was the parent body of Ryugu. Figure 3 shows the distribution of spin periods of 28 cometary nuclei that have been observed. The spin period is widely distributed up from 3.5 to 78.4 hr, with a median of about 12 hr. If Ryugu's parent comet had a spin period corresponding to the median, it would be necessary to amplify the initial angular velocity by a factor of 3.4 to bring the spin period to 3.5 hr due to water ice sublimation. The spin-up rate calculated when almost all of the

water ice sublimates in Figure 2(b) exceeds this required one. This implies that even if an amount of the water ice remains in the center, the spin-up is sufficient to cause rotation-induced deformation. In this mechanism, the rotation is slowly accelerated as the water ice sublimates. Such quasi-static rotational acceleration is thought to be desirable for the formation of a spherically symmetric spinning top shape like Ryugu (Watanabe et al. 2019).

The spin period of asteroids can be modified to be longer and shorter by the Yarkovsky–O'Keefe–Radzievskii–Paddack (YORP) effect—a radiation recoil torque affecting the rotation state of a small asteroid (Walsh 2018). The time for a km-sized body to halve or double its spin rate by this effect is on the order of ∼1 Myr (Rubincam 2000). In contrast to the YORP effect, the timescale of the spin-up due to water ice sublimation is an order of magnitude faster, about 0.1 Myr (see Figure 2(a)). Therefore, Ryugu's spinning top shape can be formed in a shorter period of time compared to the case assuming the YORP effect. However, the sublimation time strongly depends on the temperature of the cometary nucleus (see Equation (A28)). If we change only the temperature from 200 to 182 K under the same condition as in Figure 2(a), the sublimation time will exceed one million years. The sublimation time also depends on other parameters such as the initial radius of the cometary nucleus, macroporosity, size of the rocky debris, and so forth. The parameter dependence may provide constraints on the orbital evolution of Ryugu, the size of the constituent particles, and the internal macroporosity.

Cometary nuclei are thought to contain organic molecules that were formed in interstellar space as well as in the outer solar system as confirmed by infrared observations (Ehrenfreund & Schutte 2000). The organic molecules detected include CO, CO_2, CH_3OH, OCS, H_2CO, HCOOH, CH_4, and OCN^-, which account for several % with respect to H_2O (Ehrenfreund & Charnley 2000). When the water ice sublimates, although highly volatile organics listed above will sublimate with the ice, the organic residue such as refractory insoluble organic matter concentrates and is left behind on the surface of the rocky debris. In our model, the mass ratio of the rocky debris and the refractory organics left behind is equal to that of both in the initial cometary nucleus. If the water ice in the cometary nucleus initially contains ∼1 wt.% refractory organic matter, the final organic/rock-mass ratio becomes ∼0.03 on average. The organic content is consistent with the typical value of carbonaceous chondrites (Kerridge 1985). In the case of the ice sublimation scenario, the local organic content may be much higher because the organic residue concentrates on the surface of rocky debris. The local concentration may account for the extremely high organic content inferred from albedo (Potiszil et al. 2020). The organic-rich surface of comet 67P/Churyumov-Gerasimenko (Capaccioni et al. 2015) may also be explained by the sublimation-induced concentration of organic matter.

Conventional models for sublimation of volatiles from a porous cometary nucleus, though they did not consider the shrinkage of the nucleus, took into account not only the gas flow in the porous medium but also the internal thermal evolution (Mekler et al. 1990; Prialnik 1992; Prialnik & Podolak 1995). In contrast to these conventional models, our model, which assumes a uniform and constant internal temperature, may not be able to avoid criticism for being oversimplified. However, by setting the uniform and constant temperature beforehand, it is possible to answer the more general question, "What will happen if a comet experiences a given temperature and for how long?" Our approach will provide fundamental insights for examining the long-term evolution of cometary nuclei when heated.

Our calculation suggests that Ryugu was once a comet and active for the first several 10 kyr and spent the rest of its dynamic lifetime as a rubble-pile asteroid. This scenario is consistent with the dynamical evolution of modern comets in the solar system (Nuth et al. 2020). In addition, the scenario presented in this paper may be applicable to another asteroid, Bennu, which is also a spinning top-shaped rubble pile. In fact, there is some evidence that suggests that Bennu is a transitional object on its way from a comet to an asteroid (Cellino et al. 2018; Nuth et al. 2020). This is also consistent with the fact that the current spin period of Bennu (Scheeres et al. 2016, ∼4.30 hr) is shorter than that of Ryugu (Watanabe et al. 2019, ∼7.63 hr). Such facts suggest that Bennu is in an earlier evolutional stage than Ryugu, and the spin rate of Ryugu was reduced by some mechanism such as meteorite impacts (Hirata et al. 2020) or the YORP effect (Kanamaru et al. 2021).

Based on the cometary origin scenario, the following hypothesis on the origin and evolution of Ryugu is presented. The cometary nucleus that is the parent body of Ryugu has formed near the present orbit of Jupiter and Saturn, or even farther away, where water ice can coexist with silicate dust. The origin and process of the silicate dust that are incorporated into the cometary nucleus are unclear. It could be derived from the ice-coated silicate dust in the large molecular cloud from which the solar system formed or/and the silicates processed at the inner solar system. Later, it was transferred into the asteroid belt due to interactions with terrestrial planets (Hsieh 2017), then moved toward the inner asteroid belt by inward Yarkovsky drift (Bottke et al. 2015). Since the radiative equilibrium temperature in the inner asteroid belt is high enough to sublimate water ice ($\simeq 200$ K at 2.2 au), the cometary nucleus was transformed into a rubble-pile asteroid according to the process described in this paper. Eventually, the rubble-pile asteroid was injected into the orbit of the present Ryugu, probably through the ν_6 secular resonance pathway (Bottke et al. 2015).

A point that should be of concern is that the majority of near-Earth objects (NEOs) are not considered to be of cometary origin. Ryugu belongs to a group of NEOs called Apollo, of which more than 10^4 asteroids have been identified to date. Morbidelli et al. (2002) argue that the fraction of NEOs originating from comets will not exceed 10%. However, there are no studies that have quantitatively determined whether the contribution of comets is, for example, 1% or 0.1%. Even if the contribution of comets to NEOs is only 1%, we can say that more than 100 of the small bodies belonging to the Apollo asteroids are of cometary origin. This means that there is no basis for claiming that the asteroid Ryugu could not have originated from a comet.

Comet–asteroid transition objects (CATs) are small objects that were once active like comets, but have become dormant and apparently indistinguishable from asteroids (Hsieh et al. 2004). CATs are thought to provide a new insight into the solar system because of their similarities to both comets and asteroids (Hsieh 2017). Our results suggest that organic-rich, spinning top-shaped, rubble-pile objects such as Ryugu and Bennu are members of the CATs population. As demonstrated

for the Chelyabinsk meteorite (Nakamura et al. 2019), analysis of collected samples of Ryugu and Bennu in the terrestrial laboratory in a comprehensive way will further evaluate the link between rubble-pile asteroids and comets.

H.M. is supported in part by the JSPS Kakenhi (numbers 19H00820 and 20K05347), and Daiko Foundation. E.N. is supported by the Japanese Government Cabinet Office's "National University Innovation Creation Project 2020" to Okayama University. We deeply appreciate Christian Potiszil for constructive discussion and editing the manuscript. We are deeply grateful to Dr. Takashi Ito for his valuable comments on the dynamical evolution of small bodies in the solar system.

Appendix A
Formulation

Here we describe the formulation of our model that a cometary nucleus transforms to an asteroid as a result of water ice sublimation. The outline is illustrated in Figure 1. We consider a spherically symmetric, highly porous cometary nucleus with a two-layered structure consisting of the inner primitive region and the outer dust mantle, which are composed of water ice particles and rocky debris, respectively. Both the water ice particles and rocky debris are assumed to be spheres with diameters of $d_{\rm i}$ and $d_{\rm r}$, respectively. The internal temperature T is assumed to be uniform and to not vary with time. The physical quantities are uniform in the primitive region and in the dust mantle, respectively.

A.1. Definition of Parameters

Initially, the cometary nucleus consists of only the primitive region, and its radius is R_0. As the water ice sublimates, the primitive region shrinks and the rocky debris left behind accumulates on its surface. The thickness Δ of the dust mantle increases with the decrease in the radius R of the primitive region. When the water ice has completely sublimated, R becomes zero and Δ gives the final radius R_∞ of the asteroid left behind. We denote the parameter in each region with a subscript (α), where $\alpha = {\rm p}$ for the primitive region and $\alpha = {\rm m}$ for the dust mantle. The macroporosity, volume fractions of water ice particles and rocky debris, and density of the region α are denoted by $\epsilon_{(\alpha)}$, $\phi_{{\rm i}(\alpha)}$, $\phi_{{\rm r}(\alpha)}$, and $\rho_{(\alpha)}$, respectively. The relationship between the macroporosity and volume fractions is given by

$$\epsilon_{(\alpha)} = 1 - (\phi_{{\rm i}(\alpha)} + \phi_{{\rm r}(\alpha)}). \tag{A1}$$

We find $\phi_{{\rm i}({\rm m})} = 0$ because there is no water ice in the dust mantle. The density $\rho_{(\alpha)}$ of each region is given by

$$\rho_{(\alpha)} = \varrho_{\rm r}\phi_{{\rm r}(\alpha)} + \varrho_{\rm i}\phi_{{\rm i}(\alpha)}, \tag{A2}$$

where $\varrho_{\rm i}$ and $\varrho_{\rm r}$ are the material densities of the water ice particles and rocky debris, respectively. The mass fraction f of water ice in the primitive region is given by

$$f = \frac{\varrho_{\rm i}\phi_{{\rm i}({\rm p})}}{\varrho_{\rm r}\phi_{{\rm r}({\rm p})} + \varrho_{\rm i}\phi_{{\rm i}({\rm p})}} = \frac{\varrho_{\rm i}\phi_{{\rm i}({\rm p})}}{\rho_{({\rm p})}}. \tag{A3}$$

The physical quantities defined above are not independent of each other. We choose $\epsilon_{({\rm p})}$, $\epsilon_{({\rm m})}$, and f as independent input parameters that are more relevant to observation. The other quantities are determined from these independent parameters as follows. From Equation (A3), we obtain $\frac{f}{1-f} = \frac{\varrho_{\rm i}\phi_{{\rm i}({\rm p})}}{\varrho_{\rm r}\phi_{{\rm r}({\rm p})}}$. Solving this equation and Equation (A1) for $\phi_{{\rm r}({\rm p})}$ and $\phi_{{\rm i}({\rm p})}$, respectively, we obtain

$$\phi_{{\rm r}({\rm p})} = \frac{1-\epsilon_{({\rm p})}}{1 + \frac{\varrho_{\rm r}}{\varrho_{\rm i}}\frac{f}{1-f}}, \quad \phi_{{\rm i}({\rm p})} = \frac{1-\epsilon_{({\rm p})}}{\frac{\varrho_{\rm i}}{\varrho_{\rm r}}\frac{1-f}{f} + 1} \tag{A4}$$

for the primitive region, and

$$\phi_{{\rm r}({\rm m})} = 1 - \epsilon_{({\rm m})} \tag{A5}$$

for the dust mantle. The ratio $p = \rho_{({\rm m})}/\rho_{({\rm p})}$ of densities of the dust mantle to the primitive region is obtained as

$$p = \frac{\varrho_{\rm r}\phi_{{\rm r}({\rm m})}}{\varrho_{\rm r}\phi_{{\rm r}({\rm p})} + \varrho_{\rm i}\phi_{{\rm i}({\rm p})}} = \frac{1-\epsilon_{({\rm m})}}{1-\epsilon_{(p)}}\left(1 + \frac{\varrho_{\rm r} - \varrho_{\rm i}}{\varrho_{\rm i}}f\right). \tag{A6}$$

Table 1 shows the default values of input parameters. Unless otherwise noted, the values in this table are used in calculations.

Table 1
Default Values of Input Parameters Used in Calculations

Quantity	Notation	Value
Independent parameters:		
Initial radius of cometary nucleus	R_0	1.2 km
Temperature of cometary nucleus	T	200 K
Diameter of water ice particles	$d_{\rm i}$	1 μm
Diameter of rocky debris	$d_{\rm r}$	1 cm
Initial mass fraction of water ice	f	0.75
Macroporosity in primitive region	$\epsilon_{({\rm p})}$	0.8
Macroporosity in dust mantle	$\epsilon_{({\rm m})}$	0.6
Dependent parameters determined by f, ϵ_1, ϵ_2:		
Volume fraction of rocky debris in primitive region	$\phi_{{\rm r}({\rm p})}$	0.020
Volume fraction of water ice particles in primitive region	$\phi_{{\rm i}({\rm p})}$	0.180
Volume fraction of rocky debris in dust mantle	$\phi_{{\rm r}({\rm m})}$	0.4
Density of primitive region	$\rho_{({\rm p})}$	0.24 g cm^{-3}
Density of dust mantle	$\rho_{({\rm m})}$	1.20 g cm^{-3}
Ratio in densities of dust mantle to primitive region	p	5.0
Material constants:		
Material density of water ice particles	$\varrho_{\rm i}$	1.0 g cm^{-3}
Material density of rocky debris	$\varrho_{\rm r}$	3.0 g cm^{-3}

Note. The diameter of water ice particles is the typical size of interstellar dust particles. The diameter of rocky debris is the typical size of regolith on the surface of Ryugu estimated from the thermal inertia (Wada et al. 2018) and of particles ejected from an artificial impact crater on Ryugu (Wada et al. 2021). Ryugu is believed to have passed through the ν_6 resonance to its current near-Earth orbit (Bottke et al. 2015). For the temperature T, we used the radiative equilibrium temperature near ~2 au, where the ν_6 resonance exists. The water/rock-mass ratio is assumed to be 3 as expected from the solar system abundance (Hayashi 1981). The macroporosities in the primitive region and the dust mantle are based on the typical value of comets and rubble piles, respectively (Consolmagno et al. 2008). The initial radius of the cometary nucleus was chosen based on the typical size of cometary nuclei so as to become a comparable size to Ryugu after water ice sublimation.

A.2. Distribution of Vapor

A.2.1. Vapor Flow in Pores

The pores inside the cometary nucleus are filled with water vapor generated by the sublimation of water ice particles. The production rate $q_{(\mathrm{p})}$ of the water vapor per unit volume of the primitive region is given by Mekler et al. (1990) as follows:

$$q_{(\mathrm{p})} = \phi_{\mathrm{i}(\mathrm{p})} S \left(\frac{m}{2\pi k_{\mathrm{B}} T} \right)^{1/2} (P_{\mathrm{e}} - P), \tag{A7}$$

where $S = 6/d_{\mathrm{i}}$ is the surface-to-volume ratio of water ice particles, P_{e} is the equilibrium vapor pressure of water ice, P is the pressure of water vapor filling the pores, k_{B} is the Boltzmann constant, and m is the mass of a water molecule. The equilibrium vapor pressure is given by Mekler et al. (1990) as follows:

$$P_{\mathrm{e}} = 3.56 \times 10^{12} \exp\left(-\frac{6141.667}{T} \right) \mathrm{Pa}. \tag{A8}$$

However, the dust mantle does not contain water ice particles, so the production rate $q_{(\mathrm{m})}$ is naturally zero.

The flow of water vapor in the porous cometary nucleus is driven by the pressure gradient. The cometary nucleus is cold, the equilibrium vapor pressure is low, and the water vapor filling the pores is dilute. The mean free path is a few centimeters at 200 K, which is much longer than the typical size of pores (Mekler et al. 1990). Therefore, the flow can be regarded as a free molecular flow. Assuming that the region α is randomly packed with spherical particles of diameter $d_{(\alpha)}$, the flux $\boldsymbol{J}_{(\alpha)}$ of water vapor is given by Mekler et al. (1990) as follows:

$$J_{(\alpha)} = -\frac{16}{3} \left(\frac{m}{2\pi k_{\mathrm{B}}} \right)^{1/2} \frac{\epsilon_{(\alpha)}^{3/2}}{(1 - \epsilon_{(\alpha)})^{1/3}} d_{(\alpha)} \nabla \left(\frac{P}{\sqrt{T}} \right). \tag{A9}$$

The primitive region contains both water ice particles and rocky debris. Since the flux is controlled by smaller particles, the particle diameter $d_{(\mathrm{p})}$ in the primitive region can be assumed to be equal to the diameter d_{i} of water ice particles. However, since only rocky debris exists in the dust mantle, the particle diameter $d_{(\mathrm{m})}$ is equal to the diameter d_{r} of rocky debris. Although the diameter of the rocky debris assumed in this study is about the same as the mean free path of water vapor, we use the equation for a free molecular flow, because it makes the model simpler.

Let us assume that the vapor flow inside the cometary nucleus reaches steady state on the evolution timescale of the cometary nucleus. The steady flow satisfies the following continuity equation in each region:

$$\nabla \cdot \boldsymbol{J}_{(\alpha)} = q_{(\alpha)}. \tag{A10}$$

Substituting Equations (A7) and (A9) into Equation (A10) yields an equation for the pressure distribution $P(r)$, under the assumption of T being uniform. The equation results in a Laplace equation in the dust mantle. Due to the spherical symmetry, the variable of this equation is only r, a distance from the center of the cometary nucleus. This equation can be solved analytically under appropriate boundary conditions.

A.2.2. Boundary Condition

We denote the pressure distributions in the primitive region and in the dust mantle as $P_{(\mathrm{p})}(r)$ and $P_{(\mathrm{m})}(r)$, respectively. These two distributions are connected so as to satisfy the following two boundary conditions at $r = R$ (contact boundary). The first boundary condition is that the pressure is continuous; namely, $P_{(\mathrm{p})}(R) = P_{(\mathrm{m})}(R)$ (boundary condition i). The second boundary condition is that the flux is continuous; namely, $J_{(\mathrm{p})}(R) = J_{(\mathrm{m})}(R)$ (boundary condition ii). In addition, we consider a zero-flux condition at the center of the cometary nucleus ($J_{(\mathrm{p})}(0) = 0$, boundary condition iii) and zero pressure at the mantle surface ($P_{(\mathrm{m})}(R + \Delta) = 0$, boundary condition iv).

Using Equation (A9), the boundary condition (ii) is rewritten as

$$\frac{dP_{(\mathrm{p})}}{dr} = \chi \frac{dP_{(\mathrm{m})}}{dr}, \qquad (\text{at } r = R) \tag{A11}$$

where χ is a dimensionless quantity defined by

$$\chi \equiv \left(\frac{\epsilon_{(\mathrm{m})}}{\epsilon_{(\mathrm{p})}} \right)^{3/2} \left(\frac{1 - \epsilon_{(\mathrm{m})}}{1 - \epsilon_{(\mathrm{p})}} \right)^{-1/3} \frac{d_{(\mathrm{m})}}{d_{(\mathrm{p})}}. \tag{A12}$$

In this paper, we assume $d_{(\mathrm{p})} \ll d_{(\mathrm{m})}$, so $\chi \gg 1$ is valid unless the macroporosities of the primitive region and dust mantle are very different. Therefore, at the contact boundary, the magnitude of the pressure gradient in the primitive region is much larger than that in the dust mantle.

A.2.3. Analytic Solution

Solving equations for $P_{(\mathrm{p})}(r)$ and $P_{(\mathrm{m})}(r)$ together with the boundary conditions (i)–(iv), we obtain the analytical solution as follows:

$$P_{(\mathrm{p})}(r) = \left[1 - g_{R,\Delta} \frac{\sinh(r/h)}{\sinh(R/h)} \frac{R}{r} \right] P_{\mathrm{e}}, \quad (\text{for } 0 \leqslant r \leqslant R) \tag{A13}$$

$$P_{(\mathrm{m})}(r) = (1 - g_{R,\Delta}) \frac{R}{\Delta} \left(\frac{R + \Delta}{r} - 1 \right) P_{\mathrm{e}}, \quad (\text{for } R < r \leqslant R + \Delta) \tag{A14}$$

where $g_{R,\Delta}$ and h are constants, respectively, defined by

$$g_{R,\Delta} \equiv \frac{\chi(1 + \Delta/R)\tanh(R/h)}{(\Delta/h) + [\chi + (\chi - 1)\Delta/R]\tanh(R/h)},$$
$$h \equiv \frac{2\sqrt{2}}{3} \frac{\epsilon_{(\mathrm{p})}^{3/4}}{(1 - \epsilon_{(\mathrm{p})})^{1/6}} \frac{d_{(\mathrm{p})}}{\phi_{\mathrm{i}(\mathrm{p})}^{1/2}}. \tag{A15}$$

Substituting the values listed in Table 1, we obtain $h = 2.46\ \mu\mathrm{m}$.

Figure 4 shows the analytic solutions of $P_{(\mathrm{p})}(r)$ and $P_{(\mathrm{m})}(r)$. Panel (a) shows $P_{(\mathrm{p})}(r)$ and $P_{(\mathrm{m})}(r)$ near the contact boundary. The horizontal axis is the distance from the contact boundary. Here, we use $R = 1$ km and $\Delta = 1$ cm. Panel (a) shows that throughout almost the entire area of the primitive region, $P_{(\mathrm{p})}(r)$ is equal to P_{e}, indicating that a solid-vapor equilibrium has been established. However, $P_{(\mathrm{p})}(r)$ decreases rapidly in a very narrow region near the contact boundary and is connected to the pressure $P_{(\mathrm{m})}(R)$ in the dust mantle. In the dust mantle, $P_{(\mathrm{m})}(r)$ decreases slowly toward the outside and becomes zero at the surface. Panels (b) and (c), respectively, show the dependences of $P_{(\mathrm{p})}(r)$ and $P_{(\mathrm{m})}(r)$ on Δ. In panel (b), the

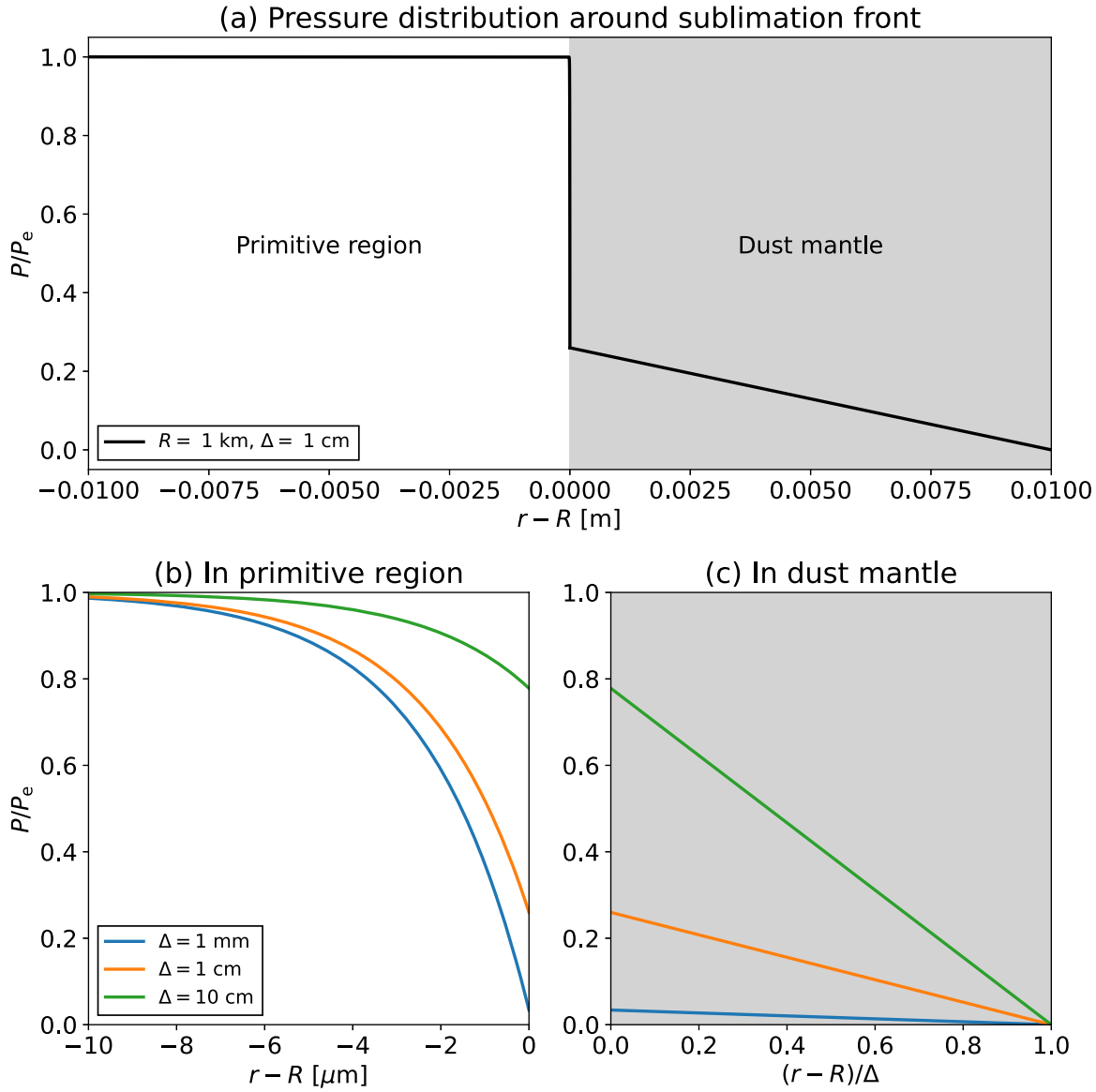

Figure 4. Analytic solution of pressure distribution $P(r)$ of water vapor in cometary nucleus. Panel (a) shows $P(r)$ near the contact boundary between the primitive region and the dust mantle in the case with $R = 1$ km and $\Delta = 1$ cm. Panels (b) and (c) show the dependence on Δ. Panel (b) is a magnified view of $P(r)$ in the primitive region, and panel (c) is in the dust mantle. The horizontal axis indicates the distance from the contact boundary, where negative values indicate the primitive region side and positive values indicate the dust mantle side. Note that the horizontal axis in panel (c) is normalized by Δ. The region corresponding to the dust mantle is filled in gray. The pressure in the vertical axis is normalized by the equilibrium vapor pressure P_e.

horizontal axis is magnified around the contact boundary. In panel (c), the horizontal axis is normalized by Δ. The thicker the dust mantle, the closer the water vapor pressure at the contact boundary is to the equilibrium vapor pressure. This trend can be understood by considering that the dust mantle acts as a lid to prevent the leakage of the water vapor. However, for any mantle thicknesses, the pressure is almost equal to P_e as one dives deeper than a few times h from the contact boundary into the primitive region. This suggests that the water ice sublimates only at the very vicinity of the contact boundary. Therefore, we refer to the contact boundary as a sublimation front in the current study.

A.3. Shrinkage of Nucleus and Dust Mantle Formation

As can be seen in Figure 4, $P_{(p)}(r)$ is not uniform in the very neighborhood of the sublimation front. The fact that the water vapor pressure varies from place to place means that the sublimation rate of water ice varies from place to place (see Equation (A7)). In other words, water ice particles closer to the sublimation front sublimate faster, so physical quantities such as the volume fraction of water ice particles cannot be strictly uniform. However, the width of this inhomogeneous region is at most a few times larger than h, which is much smaller than the size of the entire cometary nucleus. Therefore, we can assume that the physical quantities in the primitive region are uniform and that water ice sublimates only from the surface of the primitive region. In this case, the time variation of the radius R of the primitive region is given by

$$\frac{dR}{dt} = -\frac{J_{(p,sf)}}{\varrho_i \phi_{i(p)}}, \tag{A16}$$

where $J_{(\mathrm{p,sf})}$ is the value of $J_{(\mathrm{p})}$ at the sublimation front ($r = R$) and is given by

$$J_{(\mathrm{p,sf})} = 4\left(\frac{m}{\pi k_{\mathrm{B}} T}\right)^{1/2} \frac{\epsilon_{(\mathrm{p})}^{3/4}}{(1-\epsilon_{(\mathrm{p})})^{1/6}} g_{R,\Delta} \left[\frac{1}{\tanh(R/h)} - \frac{1}{R/h}\right] P_{\mathrm{e}}, \tag{A17}$$

where we used Equation (A13).

Rocky debris contained outside the primitive region accumulates on the surface of the primitive region and forms the dust mantle. From the mass conservation for the rocky debris, we obtain the following relationship between R and Δ (Watanabe 1992):

$$\frac{4\pi}{3}(R_0^3 - R^3)(1-f) = \frac{4\pi}{3}[(R+\Delta)^3 - R^3]p. \tag{A18}$$

Solving Equation (A18) for Δ, we obtain the normalized mantle thickness $k = \Delta/R_0$ as follows:

$$k = \left[x^3 + \frac{1-f}{p}(1-x^3)\right]^{1/3} - x, \tag{A19}$$

where $x = R/R_0$. The value of k with $x = 0$, $k_\infty = \left(\frac{1-f}{p}\right)^{1/3}$, gives the normalized final radius R_∞/R_0 when the cometary nucleus has transformed to an asteroid.

A.4. Spin-up

Since assuming spherical symmetry, the water vapor does not exert any reaction torque on the cometary nucleus when released. Therefore, the nucleus never starts spinning if not rotating initially. However, if the nucleus is initially rotating, the moment of inertia will change as it contracts, and its spin rate may also change. Watanabe (1992) formulated the spin-up by taking into account the angular momentum loss due to the ice sublimation and the decrease in the moment of inertia due to the contraction of the cometary nucleus. However, he assumed the case where the cometary nucleus shrinks only slightly, so his model cannot be directly applied to the drastic change where the cometary nucleus loses almost all of its water ice. Here, we modified Watanabe's formulation to apply to the case where the radius of the cometary nucleus changes significantly.

The angular momentum of the cometary nucleus is $L = I\omega$, where I is the moment of inertia of the cometary nucleus and ω is its angular velocity. Differentiating L by R, we obtain

$$\frac{1}{\omega}\frac{d\omega}{dR} = \frac{1}{I\omega}\frac{dL}{dR} - \frac{1}{I}\frac{dI}{dR}. \tag{A20}$$

The angular momentum is reduced by the amount associated with the water vapor leaking from the mantle surface. Therefore, the time variation of L is given by[4]

$$\frac{dL}{dt} = -\frac{8\pi}{3}(R+\Delta)^4 J_{(\mathrm{m,s})}\omega, \tag{A21}$$

where $J_{(\mathrm{m,s})}$ is the value of $J_{(\mathrm{m})}$ at the mantle surface ($r = R + \Delta$). From Equation (A21), we obtain

$$\frac{dL}{dR} = \frac{dL}{dt}\frac{dt}{dR} = \frac{8\pi}{3} f \rho_{(\mathrm{p})} (R+\Delta)^2 R^2 \omega, \tag{A22}$$

where we used the continuity of the water vapor flowing in the pores given by $R^2 J_{(\mathrm{p,sf})} = (R+\Delta)^2 J_{(\mathrm{m,s})}$. The moment of inertia I of the cometary nucleus including the dust mantle is given by

$$I = \frac{8\pi}{15}[\rho_{(\mathrm{m})}(R+\Delta)^5 - (\rho_{(\mathrm{m})} - \rho_{(\mathrm{p})})R^5]. \tag{A23}$$

Substituting Equations (A22) and (A23) into Equation (A20), and integrating for R from R_0 to R, we obtain the angular velocity $\omega(x)$ when the radius of the primitive region becomes $R = xR_0$, as the ratio to the initial value ω_0, as follows:

$$\frac{\omega(x)}{\omega_0} = \frac{\exp[D(x)]}{p(x+k)^5 - x^5(p-1)}, \tag{A24}$$

where $D(x)$ is a function defined by

$$D(x) \equiv \int_1^x \frac{5fx^2(x+k)^2}{p(x+k)^5 - x^5(p-1)} dx. \tag{A25}$$

When $x = 0$, the Equation (A24) gives the final spin-up rate after the water ice sublimates completely. This final spin-up rate depends only on the values of f and p, and not on the process in the middle.

Equation (A24) has the same form as the Watanabe's model, but the definition of the function $D(x)$ given by Equation (A25) differs in two respects. The first respect is the difference in the relationship between x and k (see Equation (A19)). Watanabe's model uses the approximation $k = (1-x)(1-f)/p$, which is valid only when the contraction of the cometary nucleus is sufficiently small ($x \simeq 1$ and $k \ll 1$). The second respect is that in Watanabe's model the numerator of the integrand was not $5fx^2(x+k)^2$ but $5fx^4$; namely, $(k/x)^2$ was ignored as sufficiently small for 1. In Watanabe's model, the angular momentum is assumed to be carried away when the water vapor is released outside the primitive region. However, the water vapor released from the surface of the primitive region passes through the dust mantle before being released from the cometary nucleus, and slows down its rotation. Watanabe's model is a good approximation when the contraction of the cometary nucleus is sufficiently small, but it cannot be applied to the situation where almost all the water ice sublimates, as in this study.

A.5. Numerical Scheme

Equation (A16) was integrated numerically using the fourth-order accurate Runge–Kutta method. The time step Δt is variable and is taken to be smaller as the rate of change in R is larger. Specifically, Δt was given to satisfy the following:

$$\frac{R_0/N}{\Delta t} = \left|\frac{dR}{dt}\right|, \tag{A26}$$

where N is an integer and we set $N = 10^3$ in this study. If R becomes negative, we calculate the sublimation time at which R becomes just zero by linear interpolation with the value of R at the previous time step.

The increase in the angular velocity of rotation with the shrinking of the cometary nucleus was calculated using

[4] We used the fact that the moment of inertia of a thin spherical shell with the mass M and radius R is given by $\frac{2}{3}MR^2$.

Equation (A24). The integration of $D(x)$ given by Equation (A25) was performed numerically using a package `integrate.quad()` in the Python library `SciPy`.

A.6. Parameter Dependence

The parameter dependence of the sublimation time is revealed by normalizing Equation (A16). Substituting Equation (A17) into Equation (A16), we obtain

$$\frac{dx}{d(t/\tau_{\rm sub})} \simeq -\left(\frac{1}{k}+\frac{1}{x}\right). \tag{A27}$$

Here, for $J_{\rm (p,sf)}$, we approximated $\tanh(R/h)\rightarrow 1$ because $R \gg h$, and ignored the term h/R as sufficiently small for 1. For $g_{R,\Delta}$, we used $\chi \ll 1$, and also approximated $\tanh(R/h)\rightarrow 1$ and ignored the term $\chi/(\Delta/h)$ as sufficiently small. This approximation is valid because $\chi/(\Delta/h)\sim (d_{\rm (m)}/d_{\rm (p)})/(\Delta/h)\sim d_{\rm (m)}/\Delta$, and the dust mantle is much thicker than the diameter of the rocky debris except in the very early stage of cometary nucleus evolution. From Equation (A27), we can see that the time variation of R can be scaled by a timescale $\tau_{\rm sub}$, which is defined by

$$\tau_{\rm sub} \equiv \frac{3\sqrt{2}}{16}\frac{(1-\epsilon_{\rm (m)})^{1/3}}{\epsilon_{\rm (m)}^{3/2}}\left(\frac{\pi k_{\rm B}T}{m}\right)^{1/2}\frac{\varrho_{\rm i}\phi_{\rm i(p)}}{d_{\rm (m)}}\frac{R_0^2}{P_{\rm e}}. \tag{A28}$$

This means that the sublimation time is proportional to R_0^2 and inversely proportional to $d_{\rm (m)}$ and $P_{\rm e}(T)/\sqrt{T}$.

Appendix B
Entrainment of Dust Particles

The water vapor produced by the ice sublimation can entrain small dust particles when it moves outward. The critical dust particle size, which represents the largest particle that is entrained with the escaping water vapor, is determined by the balance of forces acting on the particle: gravity, drag force, and centrifugal force (Huebner et al. 2006). Since the size of the particle we are considering is smaller than the mean free path of the escaping gas, the drag force is given by the Epstein formula as follows:

$$F_{\rm D}^{\rm (Ep)} = -\frac{4\pi}{3}c_{\rm s}a^2\rho_{\rm g}V_{\rm g}, \tag{B1}$$

where $c_{\rm s}=\sqrt{8k_{\rm B}T/\pi m}$ is the sound speed, $\rho_{\rm g}$ and $V_{\rm g}$ are the density and the velocity of the escaping gas. The mass flux of the escaping water vapor is given by $J=\epsilon^{2/3}\rho_{\rm g}V_{\rm g}$, where $\epsilon^{2/3}$ is the effective area fraction of the pores in the cometary nuclues against a given section. The centrifugal force due to the rotation of the cometary nucleus was ignored. The diameter of the largest dust particles entrained is given by a function of the distance r from the center of the cometary nucleus as follows:

$$d_{\rm max} = \frac{2c_{\rm s}}{\epsilon^{2/3}G\rho_{\rm r}}\frac{r^2J(r)}{M(r)}, \tag{B2}$$

where $J(r)$ is the water vapor flux at the position r and $M(r)$ is the mass of the cometary nucleus contained inside the position r. The entrainment of dust particles occurs between the sublimation front ($r=R$) and the surface of the cometary nucleus ($r=R+\Delta$). Therefore, by finding $d_{\rm max}$ at these two positions, we can estimate the size of the particle where entrainment occurs. We can set $J(R)=J_{\rm (p,sf)}$ and $M(R)=\frac{4}{3}\pi R^3\rho_{\rm (p)}$ at the sublimation front. At the surface of the cometary nucleus, we can set $J(R+\Delta)=J_{\rm (m,s)}$ and $M(R+\Delta)=\frac{4}{3}\pi R^3(\rho_{\rm (p)}-\rho_{\rm (m)})+\frac{4}{3}\pi(R+\Delta)^3\rho_{\rm (m)}$.

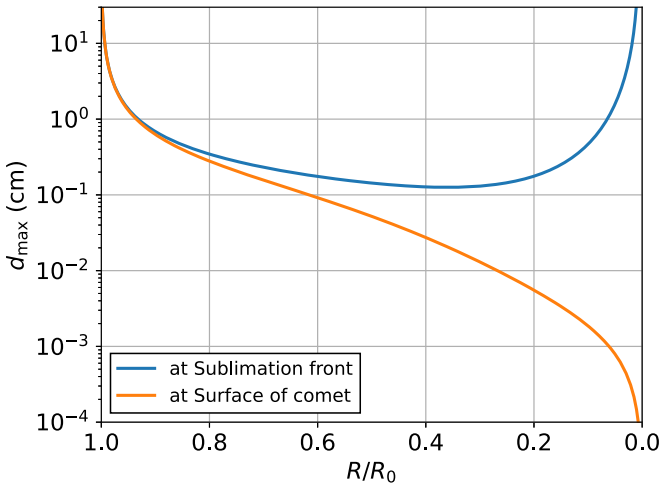

Figure 5. The diameter $d_{\rm max}$ of the largest dust particles that can be blown away by escaping water vapor at the sublimation front and at the cometary nucleus surface, respectively. The horizontal axis is the radius R of the primitive region normalized by the initial radius R_0, where $R/R_0=1$ represents the initial state and $R/R_0=0$ represents the state when the water ice is completely depleted.

Figure 5 shows the variation of $d_{\rm max}$ during the water ice is sublimating from the cometary nucleus at respective positions of the sublimation front and the cometary nucleus surface. In the early stage of contraction, the water vapor is released from the cometary nuclues surface so severely that even dust particles as large as 10 cm can be blown away. The water vapor flux decreases as the thickness of the dust mantle increases, so $d_{\rm max}$ decreases with time at both positions. However, as the position of the sublimation front approaches the center of the cometary nucleus, the gravity at the position weakens, and $d_{\rm max}$ at the sublimation front begins to increase. By contrast, $d_{\rm max}$ at the cometary nucleus surface decreases monotonically with time as the water vapor flux decreases. Therefore, in the late stage of ice sublimation, the intermediate-sized particle that is blown away at the sublimation front may stop before reaching the cometary nucleus surface. Nevertheless, it turns out that dust particles smaller than $\sim$10 μm can be ejected from the cometary nucleus in almost all evolutionary stages.

ORCID iDs

Hitoshi Miura https://orcid.org/0000-0001-8891-1658
Eizo Nakamura https://orcid.org/0000-0003-4399-9443
Tak Kunihiro https://orcid.org/0000-0001-5605-1227

References

Bottke, W. F., Vokrouhlický, D., Walsh, K. J., et al. 2015, Icar, 247, 191
Capaccioni, F., Coradini, A., Filacchione, G., et al. 2015, Sci, 347, aaa0628
Cellino, A., Bagnulo, S., Belskaya, I. N., & Christou, A. A. 2018, MNRAS, 481, L49
Consolmagno, G., Britt, D., & Macke, R. 2008, ChEG, 68, 1
Ehrenfreund, P., & Charnley, S. B. 2000, ARA&A, 38, 427
Ehrenfreund, P., & Schutte, W. 2000, AdSpR, 25, 2177
Fujiwara, A., Kawaguchi, J., Yeomans, D. K., et al. 2006, Sci, 312, 1330
Hayashi, C. 1981, PThPS, 70, 35
Hirata, N., Morota, T., Cho, Y., et al. 2020, Icar, 338, 113527

Hsieh, H. H. 2017, RSPTA, 375, 20160259
Hsieh, H. H., Jewitt, D. C., & Fernández, Y. R. 2004, AJ, 127, 2997
Huebner, W. F., Benkhoff, J., Capria, M., et al. 2006, in Heat and gas diffusion in comet nuclei, International Space Science Institute (Noordwijk: ESA)
Kanamaru, M., Sasaki, S., Morota, T., et al. 2021, JGRE, 126, e06863
Kerridge, J. F. 1985, GeCoA, 49, 1707
Lauretta, D. S., DellaGiustina, D. N., Bennett, C. A., et al. 2019, Natur, 568, 55
Mekler, Y., Prialnik, D., & Podolak, M. 1990, ApJ, 356, 682
Michel, P., Ballouz, R. L., Barnouin, O. S., et al. 2020, NatCo, 11, 2655
Michel, P., Benz, W., Tanga, P., & Richardson, D. C. 2001, Sci, 294, 1696
Morbidelli, A., Bottke, W. F., Froeschlé, C., & Michel, P. 2002, in Asteroids III, ed. W. F. B. A. Cellino, Jr., P. Paolicchi, & R. P. Binzel (Tucson, AZ: Univ. of Arizona Press)
Nakamura, E., Kunihiro, T., Ota, T., et al. 2019, PJAB, 95, 165
Nakamura, E., Makishima, A., Moriguti, T., et al. 2012, PNAS, 109, E624
Nuth, J. A., Abreu, N., Ferguson, F. T., et al. 2020, PSJ, 1, 82
Okada, T., Fukuhara, T., Tanaka, S., et al. 2020, Natur, 579, 518
Potiszil, C., Tanaka, R., Kobayashi, K., Kunihiro, T., & Nakamura, E. 2020, AsBio, 20, 916
Prialnik, D. 1992, ApJ, 388, 196
Prialnik, D., & Podolak, M. 1995, Icar, 117, 420
Rubincam, D. P. 2000, Icar, 148, 2
Samarasinha, N. H. A. M. B. E., Belton, M. J. S., & Jorda, L. 2019, PDSS, https://pds.nasa.gov/ds-view/pds/viewCollection.jsp?identifier=urn%3Anasa%3Apds%3Acompil-comet%3Anuc_rotation&version=1.0
Scheeres, D., Hesar, S., Tardivel, S., et al. 2016, Icar, 276, 116
Wada, K., Grott, M., Michel, P., et al. 2018, PEPS, 5, 82
Wada, K., Ishibashi, K., Kimura, H., et al. 2021, A&A, 647, A43
Walsh, K. J. 2018, ARA&A, 56, 593
Watanabe, J. 1992, PASJ, 44, 163
Watanabe, S., Hirabayashi, M., Hirata, N., et al. 2019, Sci, 364, 268